

On the atomic structure of Pt(111)/ γ -Al₂O₃(111) interfaces and the changes in their interfacial energy with temperature and oxygen pressure

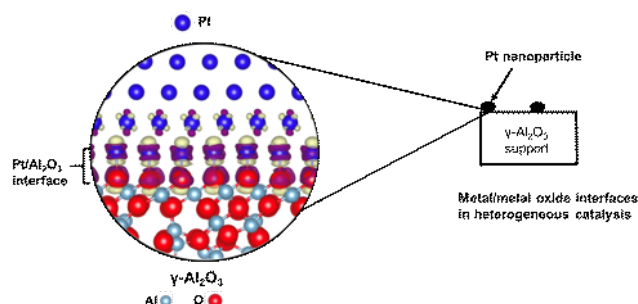
K. Oware Sarfo¹, A. L. Clauser², M.K. Santala², L. Árnadóttir^{1,*}

¹School of Chemical, Biological, and Environmental Engineering, Oregon State University, Corvallis, OR USA

²School of Mechanical, Industrial, and Manufacturing Engineering, Oregon State University, Corvallis, OR USA

[*liney.arnadottir@oregonstate.edu](mailto:liney.arnadottir@oregonstate.edu)

TOC graphics



Abstract

Metal/metal-oxide interfaces are important in many applications including metal coatings, sensing, and catalysis. Here we investigate and predict the structure and chemical bonding of the interface between γ -Al₂O₃ and Pt using density functional theory. Previous high-resolution transmission electron microscopy studies showed atomically flat interfaces between the (111) planes of Pt and γ -Al₂O₃; this interfacial orientation is studied herein. A simulated temperature-pressure equilibrium configuration diagram shows how the stability of the interfaces changes with temperature and oxygen pressure. Of the three interfacial terminations (O, Al, Al₂) the oxygen-terminated γ -Al₂O₃ (111) is the most stable at atmospheric conditions. The stability of this interface is attributed to the strong electrostatic interaction between the Pt and the oxygen atoms at the oxygen-terminated interface. This work provides essential insights into the atomic structure and the origins of the interactions at the interface between transition metals and metal oxides, as well as interfacial configuration at a range of conditions.

Keywords: Interface, gamma-Al₂O₃, Pt nanoparticles, Density Functional Theory

1. Introduction

Metal/metal-oxide interfaces are present in many material applications such as microelectronics, dentistry, photovoltaics, and thermal barrier coatings.[1-4] Several theoretical and experimental studies have been devoted to understanding the relationship between processing,

structure, and properties of interfaces and the effects of oxygen activity on interfacial structure and stability.[5-10] For example, sessile drop experiments have demonstrated the effect of oxygen pressure on the wetting behavior, interfacial energy, and work of adhesion at molten-metal/solid-metal-oxide interfaces.[11-13] Oxygen activity has also been shown to shift the relative interfacial energies of liquid-Cu/solid-MgO interfaces, which is attributed to changes in the chemistry of the interfaces.[14, 15]

Metal/ Al_2O_3 interface studies go back decades and have mostly focused on metal/ $\alpha\text{-Al}_2\text{O}_3$ interfaces due to the importance of $\alpha\text{-Al}_2\text{O}_3$ as structural ceramic, while metal/ $\gamma\text{-Al}_2\text{O}_3$ interfaces have been studied in less depth.[16-20] The atomically flat, non-stoichiometric $\alpha\text{-Al}_2\text{O}_3(0001)$ facet can have an oxygen or two different types of aluminum terminations but the stability of the different terminations depends on many parameters including the nature of the metal and oxygen potentials.[16, 21-23] *Ab initio* thermodynamic studies of Nb/ $\alpha\text{-Al}_2\text{O}_3(0001)$ interface have found the O-terminated interface has the highest work of separation and the Al/ $\alpha\text{-Al}_2\text{O}_3(0001)$ interface is oxygen terminated except at the lowest oxygen potentials.[16, 24] The Ag/ $\alpha\text{-Al}_2\text{O}_3(0001)$ interface is Al terminated up to a chemical potential of ~ 1.5 eV (with reference to ambient oxygen gas) but above 1.5 eV the O-terminated interface is more stable. Similarly, the O-terminated interface of Pt(111)/ $\alpha\text{-Al}_2\text{O}_3(0001)$ was found to be the most stable at experimentally accessible temperatures and oxygen pressures by combined HRTEM and *ab initio* thermodynamics approach [19].

Here, we employ density functional theory (DFT) to investigate the stability of different chemical terminations of the Pt(111)/ $\gamma\text{-Al}_2\text{O}_3(111)$ interface. The $\gamma\text{-Al}_2\text{O}_3(111)$ facet has a polar surface which can be terminated by a layer of aluminum (Al), layer of oxygen (O) or two layers of aluminum (Al_2). We use *ab initio* thermodynamics, previously presented by Reuter and Scheffler,[23] to determine the interfacial structure and relative stability for different $\gamma\text{-Al}_2\text{O}_3$ terminations with Pt, through calculations of interfacial energies as a function of temperature and oxygen pressure.

The choice of the interfacial orientation for this study is based on interfaces with Pt(111)|| $\gamma\text{-Al}_2\text{O}_3(111)\gamma$; Pt[$\bar{1}\bar{1}0$]| $\gamma\text{-Al}_2\text{O}_3[1\bar{1}0]$ orientation by HRTEM, Fig. 1. [25] This orientation relationship will hereafter be referred to as Pt(111)/ $\gamma\text{-Al}_2\text{O}_3(111)$ for brevity. The HRTEM specimen shown in Fig. 1 was produced *via* high-energy ion implantation of Pt into the near surface region of a sapphire ($\alpha\text{-Al}_2\text{O}_3$) wafer. The implantation partially amorphized the $\alpha\text{-Al}_2\text{O}_3$, and subsequent thermal annealing in air at 800°C for 500 h resulted in Pt nanoparticles embedded in $\gamma\text{-Al}_2\text{O}_3$. Details of processing and characterization have been reported elsewhere.[25]

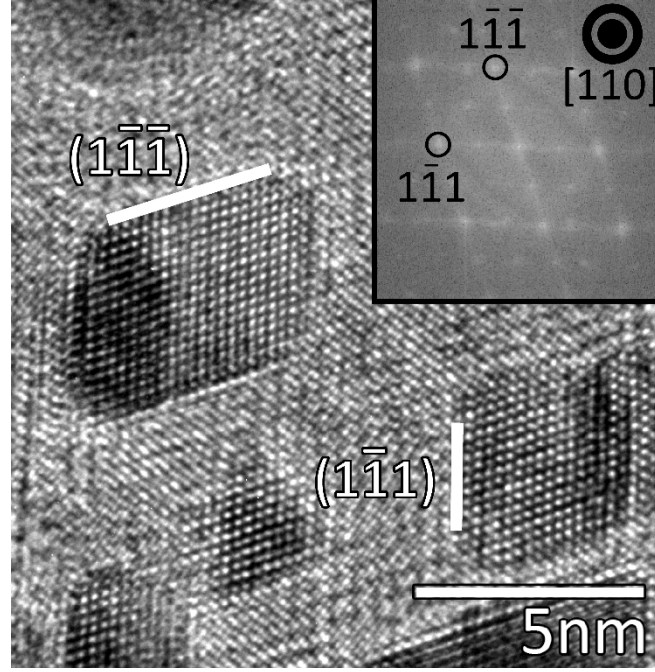


Fig. 1. HRTEM phase contrast image showing sharply faceted Pt nanoparticles in γ - Al_2O_3 . The fast Fourier transform (FFT) of the image region (inset) is consistent with the orientation relationship $\text{Pt}(111)\parallel\gamma\text{-Al}_2\text{O}_3(111)$; $\text{Pt}[1\bar{1}0]\parallel\gamma\text{-Al}_2\text{O}_3[1\bar{1}0]$. The Pt $\{111\}$ spots labeled in the FFT coincide with the $\gamma\text{-Al}_2\text{O}_3$ 222. White lines are parallel to the $\{111\}$ faceted interfaces.

This interfacial orientation has also been observed on faceted $\gamma\text{-Al}_2\text{O}_3$ inclusions formed in Cu by internal oxidation.[26] For Pt in $\gamma\text{-Al}_2\text{O}_3$, this interfacial orientation relationship has a good in-plane lattice match where the Pt-Pt nearest-neighbor spacing is only 0.31% larger than the average O-O nearest-neighbor spacing in the $\gamma\text{-Al}_2\text{O}_3$ $\langle 110 \rangle$ directions, so small misfit strain contributions to the interfacial energy are expected.

The possible interfacial interactions are limited by the orientation relationship between the matrix and the nanoparticle. The stability of the $\text{Pt}(111)/\gamma\text{-Al}_2\text{O}_3(111)$ interface could not have been inferred from the properties of the individual components since the solid-solid heterointerfaces are substantially different from surfaces of each component in contact with a gas phase. The appearance of faceted (111) interfaces does not conflict with $\gamma\text{-Al}_2\text{O}_3(111)$ surfaces having substantially higher surface energy than both (100) and (110) surfaces in vacuum.[27] The equilibrium shape of clean Pt has been shown to have little difference in the relative surface energy of (111) and (001) surfaces at 1200°C and at that temperature the surface energies are only a few percent lower than other arbitrary orientations.[28] As context for the structural and electronic study of the $\text{Pt}/\gamma\text{-Al}_2\text{O}_3$ interface, the surface energy of three low index facets of $\gamma\text{-Al}_2\text{O}_3$ (111), (110), and (100) are reported in the supplementary document as a function of oxygen pressure.

2. Calculation Methods

2.1. Computational details

All calculations herein were based on DFT as implemented in the Vienna Ab Initio Simulation Package (VASP)[29-32] using generalized gradient approximation (GGA) with the Perdue-Burke-Erzerhof (PBE) exchange correlation functional.[33] The cut-off energy for the plane wave basis set was 450 eV and core electrons were described using projector augmented wave (PAW) method.[34, 35] Ground state configurations were minimized until total forces on each atom were less than 0.05 eV/Å. A 3x3x1 Monkhorst-Pack[36] uniform k -point sampling for the integration of the Brillouin zone was enough to ensure convergence of the surface energies of the models to within 0.001 J/m².

The structure of γ -Al₂O₃ is commonly described as a defective spinel with cubic close packed oxygen anions forming tetrahedral and octahedral interstices where Al ions are randomly distributed but not fully occupied to satisfy the γ -Al₂O₃ stoichiometry.[37-39] The exact positions and distributions of the aluminum cations and unoccupied oxygen interstices (Al vacancies) are unresolved and depend on the preparation conditions of γ -Al₂O₃. [38, 40] This lack of consensus regarding the structure of the γ -Al₂O₃ can affect our capability to predict and compare these interfacial structures directly to high resolution TEM images of the interface. A commonly used model for γ -Al₂O₃ is the non-spinel model proposed by Digne *et al.*[41] which is based on the work by Krokidis *et al.*[42] who simulated a wide range of distributions of Al cations in oxygen interstices and found that the most stable structure has 25% tetrahedral aluminum. The Digne model is used herein.

The optimized lattice parameters for γ -Al₂O₃ bulk structure were $a = 5.536$ Å, $b = 8.328$ Å and $c = 8.018$ Å, consistent with previous experiment ($a = 5.652$ Å, $c = 7.871$ Å)[43] and theory ($a = 5.587$ Å, $b = 8.413$ Å, $c = 8.068$ Å).[44, 45] A (1x1) unit cell separated by a total of ~20 Å vacuum layer in the z-direction was used for the surface energy calculations. Different terminations were created by removing surface atoms from the top of the slab and freezing the bottom two Al₂O₃ layers keeping the bottom termination constant for consistent comparison. The number of different terminations presented in Fig. 2 depends on the number of non-equivalent layers in the unit cell for each surface orientation. The model structures with non-stoichiometric terminations, comprising terminations B and C for (100) and O and Al₂ for (111) are characterized by the excess or deficiency of oxygen atoms with respect to the stoichiometry of γ -Al₂O₃. The (100) and (110) surface terminations are labeled using letters A, B and C while the (111) surface terminations nomenclature are based on the species that terminate the surface, similar to the naming schemes for polar metal oxides.[17, 19, 46-49] The surface energy was converged for slab thickness for the three surface orientations and presented in the Supplementary-Table SI. The surface energies converged to within ~0.02 J/m² with six layers for the γ -Al₂O₃(111) surface which was used for interfacial calculations herein.

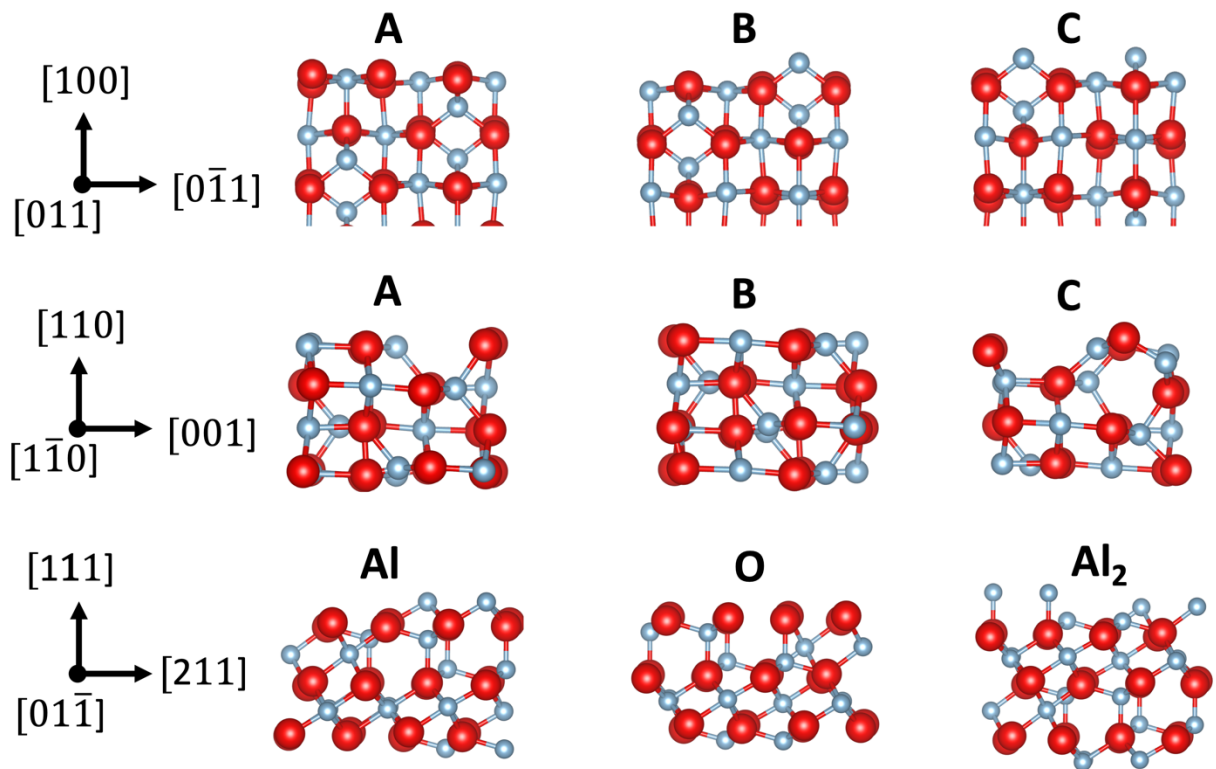


Fig. 2. Side views of three unrelaxed low index planes of γ - Al_2O_3 showing different terminations (labelled A, B, C for (100) and (110) for which the terminating layers contain both O and Al but Al, O, Al_2 for (111) where the terminating surface layer are the all same element). The stoichiometric terminations include A for (100), all three terminations of (110) and Al for (111). Al cations and O anions are shown as small light grey spheres and large red spheres respectively.

The lattice constant used for Pt was 3.98 Å, consistent with previous calculations (3.99 Å-PBE)[50, 51] and experiment (3.92 Å).[52] A five-layer Pt slab was adequate to converge the surface energy to $<0.06 \text{ J/m}^2$. The surface energies for 3-6 layer Pt slabs are presented in the Supplementary-Table SII.

The interfacial calculations were done using a supercell model shown in Fig. 3 consisting of a 5-layer Pt (111) slab interfacing with six layers of γ - Al_2O_3 (111) slab at a specified surface termination ($\text{Al}/\text{O}/\text{Al}_2$). The periodic images are separated by $\sim 20 \text{ Å}$ of vacuum. The γ - Al_2O_3 -vacuum interface is kept frozen for consistency.

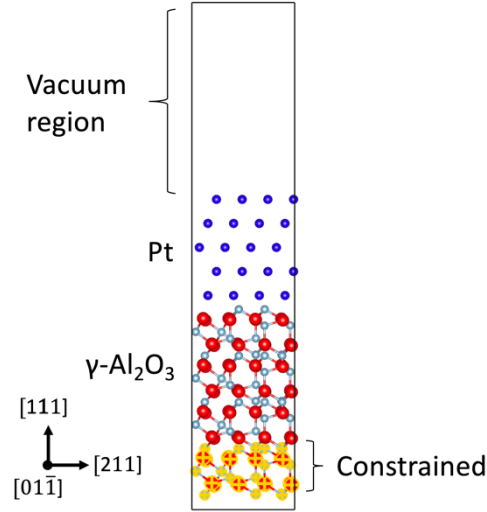


Fig. 3. Schematic of the structure used in the DFT calculations of the interface, containing a Pt (111) slab on top of a γ - Al_2O_3 (111) slab, forming an interface at the point of contact between the two slabs. A 20 Å of vacuum separates the Pt and the periodic image of the γ - Al_2O_3 slab in the in z-direction. Al, Pt cations and O anions are shown as small light grey, small blue and large red spheres respectively, this color scheme is used throughout this paper.

Calculations were performed using different initial positions of the Pt slab relative to the Al and O atomic positions on the γ - Al_2O_3 surface to assess whether the calculated interfacial configuration reflected a local or global energy minimum as presented in Fig. S1 in the Supplementary material. For Al-terminated interface, calculations were done for initial configurations where the terminal Al atoms lined up with top and hollow site on the Pt (111) interface. For the O terminated interface, the energy of the interfaces for Pt atoms above the top sites, the bridge sites and the hollow sites of interfacial O atoms were calculated and for the Al_2 terminated interface the configurations where the Al is above top sites and mostly in line with the hollow sites of Pt interfacial atoms was calculated.

Electron transfer at the interface was studied by Bader charge analysis[53-56] and visualized through charge density difference plots (CDD) using Vesta.[57] Charge density difference, $\Delta\rho$, was calculated by comparing the charge density of the total structure($\rho_{\text{Pt}/\text{Al}_2\text{O}_3}$), Pt(ρ_{Pt}), and Al_2O_3 ($\rho_{\text{Al}_2\text{O}_3}$) by:

$$\Delta\rho = \rho_{\text{Pt}/\text{Al}_2\text{O}_3} - \rho_{\text{Pt}} - \rho_{\text{Al}_2\text{O}_3} \quad (1)$$

2.2. Surface and interfacial thermodynamics

The surface energy, σ_s , was calculated using the *ab initio* thermodynamics approach developed by Reuter and Scheffler,[23] and Bergemayer *et al.*,[48] where temperature and pressure dependence are included through the chemical potentials of oxygen and aluminum in Eq. (2).

$$\sigma_S(T, pO_2) = \frac{1}{2A} E_{slab} - \frac{1}{6A} N_O \mu_{Al_2O_3} + \frac{1}{A} \left(\frac{3}{2} N_{Al} - N_O \right) \left[\frac{kT}{4} \log(pO_2) - \frac{1}{3} \mu_{Al} - \frac{1}{6} \Delta G_{Al_2O_3}^f(T) \right] \quad (2)$$

where E_{slab} represent the total energy of the slab, k , Boltzmann's constant and A , the area of the slab. N_i and μ_i represent the number of atoms and chemical potential of Al, O, Pt and Al_2O_3 respectively. $G_{Al_2O_3}^f$ is the Gibbs free energy of Al_2O_3 formation, T temperature (K) and pO_2 the partial pressure of oxygen (atm). The lowest surface energy for a given temperature and oxygen pressure is taken to be the most thermodynamically stable surface.[23, 48]

The interfacial energies, σ_I were determined using the *ab initio* thermodynamic method described previously[16, 17, 19, 23] and summarized in Eq. (3).

$$\sigma_I(T, pO_2) = \frac{1}{A} E_{tot} - \sigma_{Pt/vac} - \sigma_S - \frac{1}{A} N_{Pt} \mu_{Pt} - \frac{1}{3A} N_O \mu_{Al_2O_3} + \frac{1}{A} \left(\frac{3}{2} N_{Al} - N_O \right) \left[\frac{kT}{4} \log(pO_2) - \frac{1}{3} \mu_{Al} - \frac{1}{6} \Delta G_{Al_2O_3}^f(T) \right]. \quad (3)$$

where E_{tot} and $\sigma_{Pt/vac}$ are the total energy of the interfacial structure and the surface energy of the Pt(111) slab respectively. The derivations for surface and interfacial energies are given in the supplementary information.

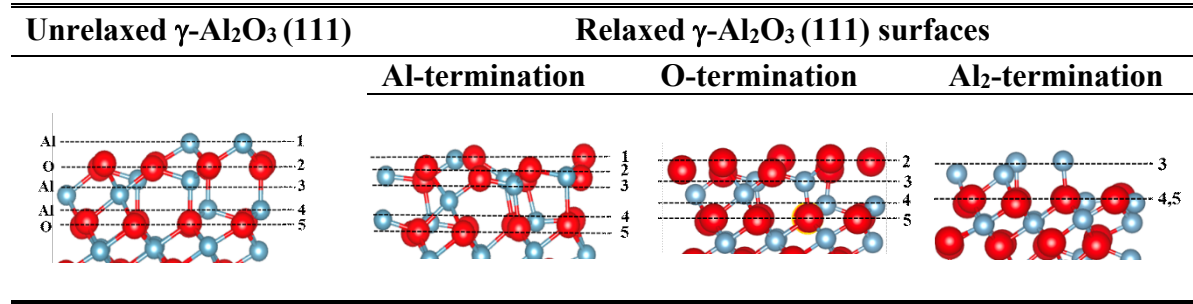
3.0. Results and Discussions

3.1. Surface study of γ - Al_2O_3 (111)

The structure of the γ - Al_2O_3 surface was studied to determine the changes in the geometry relative to the bulk. Here we focus on the γ - Al_2O_3 (111) orientation at the interface based on the previously mentioned experiments.

The γ - Al_2O_3 (111) surface has three distinct and polar surface terminations constituted by just one type of element (Al or O); an Al termination with a single or double layer of aluminum, and an O termination. The unrelaxed structure and the changes in interlayer distance in the z direction after energy relaxation for the different terminations are shown in Table 1. The Al termination showed the largest relaxation or 94.1% reduction in the interplanar distance between the terminating Al atoms (Table 1 - layer 1) and the subsurface O atoms (Table 1 - layer 2) which is similar to calculations of Al-terminated α - Al_2O_3 , where the Al-O interplanar distance decreased by 77.0%.[58] This relaxation can be ascribed to the electrostatic interactions between Al and O subsurface atoms to reduce the excess surface charges on the Al atoms.

Table 1. Side view of different terminations of a γ - Al_2O_3 (111) surface after relaxation. The numbers refer to the atomic layer positions of Al and O atoms with reference to the unrelaxed bulk structure.



For the O-terminated surface, the O-Al distance between layers 2 and 3 increases by 15.1% upon relaxation (Table 1 - layer 3), similar to O-terminated α - Al_2O_3 (0001) surface[59] and the Al atoms in layer 3 shift slightly inwards closer to layer 4 reducing the interlayer distance between layer 3 and layer 4 by only 7.8% .

Table 2. Surface relaxations of the different terminations given in % relative to the interplanar distance in the unrelaxed geometry as illustrated in Tab. 1. Negative sign signifies a reduction in the interplanar distance. The percentages were determined from the average interplanar distances.

Surface termination	Interlayer relaxations in %			
	layers 1-2	layers 2-3	layers 3-4	layers 4-5
Al termination	-94.1	-21.6	+57.3	-49.9
O termination		+15.1	-7.8	+11.6
Al_2 termination			+82.9	-100.0

The Al_2 -terminated surface is terminated by two layers of Al atoms similar to metal oxide terminations described as metal-rich or oxygen deficient surfaces.[17, 60] The Al atoms on the surface (Table 1 - layer 3) relax outward by 82.9% while the Al atoms in layer 4 shift inwards increasing the interlayer distance between the two terminating Al layers. This suggests a stronger Al-O interaction between the Al atoms in the second layer (Table 1 - layer 4) and the oxygen atoms beneath (Table 1 - layer 5).

The surface energies were estimated using *ab initio* thermodynamics as a function of oxygen pressure according to Eq. (2) at experimental annealing temperature (1100 K). The stability order for γ - Al_2O_3 surface orientations at atmospheric pressure of oxygen ($p\text{O}_2 = 0.21$ atm) is (100) > (110) > (111) (see supplementary data Fig. S2-S4).

The surface energies of the three surface terminations of γ - Al_2O_3 (111) are plotted as a function of oxygen pressures at 1100 K in Fig. 4. The Al-terminated surface energy is constant and the lowest of the three in an intermediate range of oxygen pressures while the surface energy of O- and Al_2 -terminated surfaces decrease and increase with increasing oxygen pressure, respectively.

At atmospheric oxygen pressure ($pO_2 = 0.21$ atm) and 1100 K the Al-terminated surface is predicted to be the most stable surface termination.

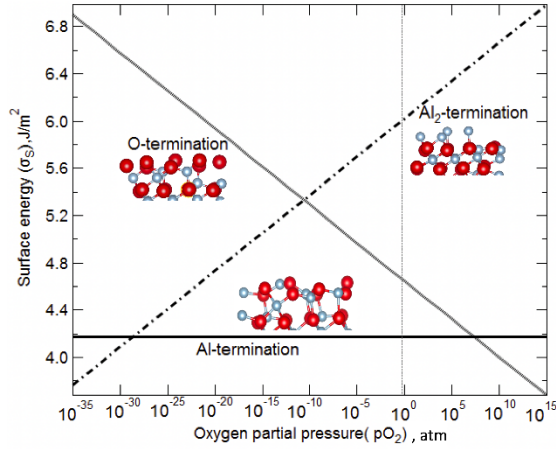


Fig. 4. Surface energy of the Al, O and Al₂ terminations (with insets) of the γ -Al₂O₃ (111) as a function of partial pressure of oxygen at 1100 K. Oxygen pressure at atmospheric conditions, ($pO_2 = 0.21$ atm) is shown as a dotted vertical line.

3.2. Interfacial study of Pt(111)|| γ -Al₂O₃(111)

The most stable configurations of each of the three interfacial terminations and the atomic structure at the interface, in comparison with the unrelaxed structure, are presented in Table 3.

Interlayer relaxations in the Pt slab for all three interfacial structures are less than 3% relative to the bulk, but the relaxations are largest closest to the interface (Table 3 layers ii-iii). Interlayer relaxations for the different Pt/ γ -Al₂O₃ terminations relative to the unrelaxed structure are listed in Table 4.

The Al-terminated interface has a 78.1% reduction in interlayer distance between the Al and O layers (Table 3 layers 1-2) resulting in nearly coplanar Al and O similar to the relaxation of the Al-terminated surface. Like the surface, interfacial relaxations at the O-terminated interface leads to an increase in the interlayer distance between the surface O atoms and the subsurface Al atoms (Table 3 layers 2-3). The Al₂-terminated interface relaxes essentially into a single plane of Al atoms with an 82.3% reduction in interlayer distance at the Pt/ γ -Al₂O₃ interface (Table 3 layers 3-4) in contrast to the Al₂-terminated surface where the distance between outermost and second Al layers increased after relaxation.

Table 3. Side (top) and cross-sectional (bottom) views of the lowest energy configurations of the Pt/ γ -Al₂O₃ interfaces for Al, O and Al₂-terminations. Pt, O and Al atoms shown in blue, red and grey respectively.

**Unrelaxed Pt(111)/ γ -
Al₂O₃ (111)**

Relaxed Pt(111)/ γ -Al₂O₃ (111) surfaces

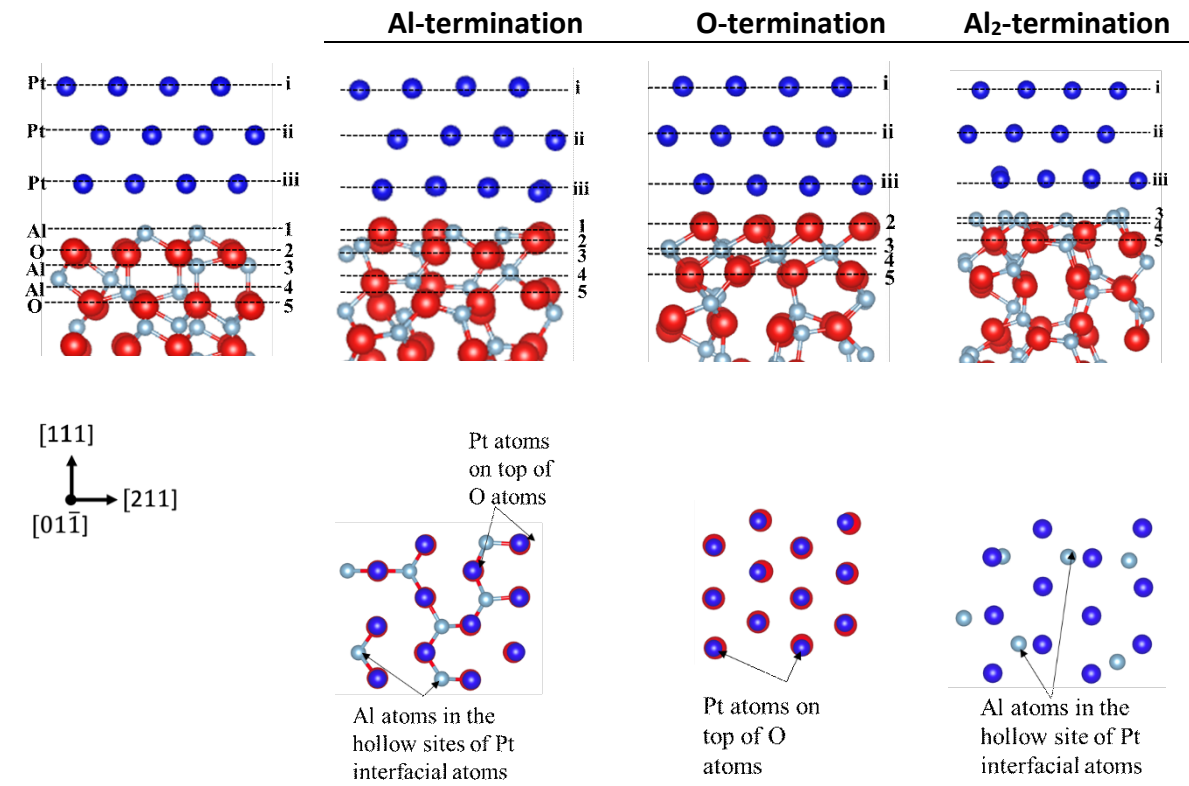


Table 4. Comparison of interfacial relaxations of the different Al₂O₃ terminations given in % relative to the interplanar distance in the unrelaxed geometry as illustrated in Table 3. A negative sign signifies a reduction in the interplanar distance. The percentages were determined from the average interplanar distances.

Interlayer relaxations in % relative to unrelaxed structure									
Interface termination	Pt		Al ₂ O ₃				Interfacial distance, Å		
	layers	i-ii	ii-iii	1-2	2-3	3-4	4-5	Pt-Al	Pt-O
Al termination		+0.2	+1.6	-78.1	-15.3	+44.0	+8.4	2.1	2.3
O termination		-0.8	-0.3		+15.4	-85.4	-63.1		1.9
Al ₂ termination		+1.2	+2.3			-82.3	+68.0	2.0	

For both the Al and O terminations, the interfacial O atoms align with the Pt top sites at the interface, separated by ~2.0 Å, while for the Al₂-terminated interface, the Al atoms line-up with the Pt hollow sites (Table 3-bottom). The location of the Pt atoms relative to the O atoms at the Al and O interfaces and the short distances between them are indicative of strong Pt-O interactions

consistent with Hemmingson and Campbell [22] who showed that metal-oxygen interactions dominate interfacial interactions

The interfacial energies for the different interfacial terminations at 1100 K as a function of oxygen pressure are presented in Fig. 5. At very low oxygen pressures ($pO_2 \leq 10^{-10.5}$ atm), the Al_2 -terminated interface is the most stable configuration but this transitions to the Al-terminated interface, and then O-terminated interface from $pO_2 = 10^{-7.5}$ atm onwards. The interfacial energy of the O-terminated interface decreases with increasing oxygen pressure while the Al_2 -terminated interface and Al-terminated interface increases and remains independent of oxygen pressures respectively.

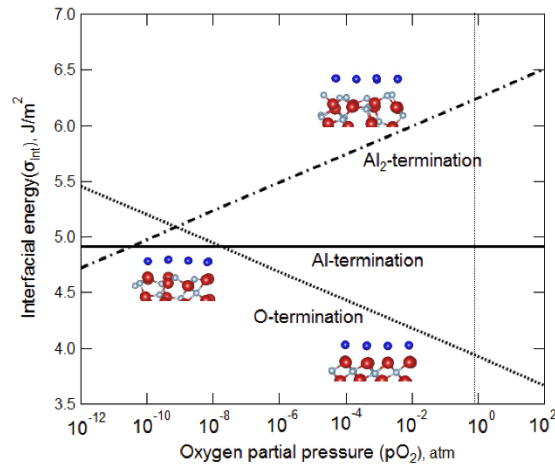


Fig. 5. Interfacial energy versus partial pressure of oxygen at 1100 K for the Al, O, and Al_2 terminations (with insets) of the Pt/ γ - Al_2O_3 (111) interface. Oxygen pressure at atmospheric conditions is shown as a dotted vertical line.

An equilibrium configuration diagram, based on the interfacial energy calculations, is presented in Fig. 6 and maps the termination of the interface as a function of temperature and oxygen pressure. At $pO_2 = 0.21$ atm and $T = 298$ K (point ‘STP’ on Fig. 6), the O-terminated Pt/ γ - Al_2O_3 interface is the most stable in agreement with Ophus et al.[19] for the Pt(111)/ α - Al_2O_3 (0001) interface at atmospheric conditions.

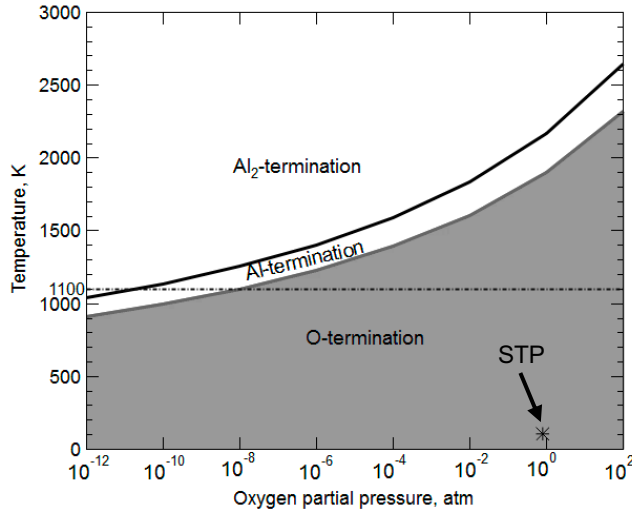


Fig. 6. Temperature-pressure equilibrium configuration diagram for the Al, O and Al₂ interfaces of Pt/γ-Al₂O₃. Oxygen pressure at standard conditions ($p_{O_2} = 0.21$ atm, $T = 298$ K) is shown as point 'STP'. The temperature beyond which γ-Al₂O₃ transitions into δ-Al₂O₃ is indicated by the dotted horizontal line through 1100 K.[57]

At $p_{O_2} = 0.21$ atm the O-terminated interface is the most stable up to 1900 K but above 1100 K the γ-Al₂O₃ phase transitions into δ-Al₂O₃ phase so temperature considerations should not go beyond 1100 K for the Pt/γ-Al₂O₃ interface.[61]

3.2.1. Chemical bonding at interface

Electron charge density difference and Bader charge analysis were used to analyze charge transfer and bonding at the metal/metal oxide interface (Fig. 7). At the O-terminated interface, the terminating O atoms align with the atop sites of the Pt surface (see Fig. 7(a)) gaining ~ 0.3 e, whereas Pt atoms with which they interact lose ~ 0.4 e. This suggests charge transfer from Pt to O atoms which provides the basis for strong electrostatic interaction at the interface.

At the Al₂-terminated interface, the Al atoms sit in the hollow sites of the Pt slab. Fig. 7(b) shows a broad electron cloud near the Pt atoms at the interface with a net gain of ~ 0.4 e while the Al atoms at the interface are depleted in electron density by ~ 0.8 e characteristic of metallic bonding between the metal cations. [17]

The Pt atoms interact with both O and Al atoms at the Al-terminated Pt/γ-Al₂O₃ interface (see Tab. III). Pt atoms located directly on top of O atoms are depleted in electron density by ~ 0.3 e, whereas the O atoms with which they interact gain ~ 0.3 e slightly less than the charge transfer for the O termination, suggesting a slightly weaker Pt-O interaction at the Al-terminated interface. The Al atoms at the Al-terminated interface are aligned with the hollow sites of the Pt plane (see Fig. 7(c)) just like Al atoms at the Al₂ interfacial termination. The Pt atoms have a net gain of electrons of approximately 0.5 e while the Al atoms with whom they interact lose electrons constituted by a combination of cation-anion electrostatic contributions and metallic bond contributions. This suggests similar but weaker metal-metal interaction than the Al₂ interfacial termination in agreement with the observation by Siegel[20] for Al/α-Al₂O₃.

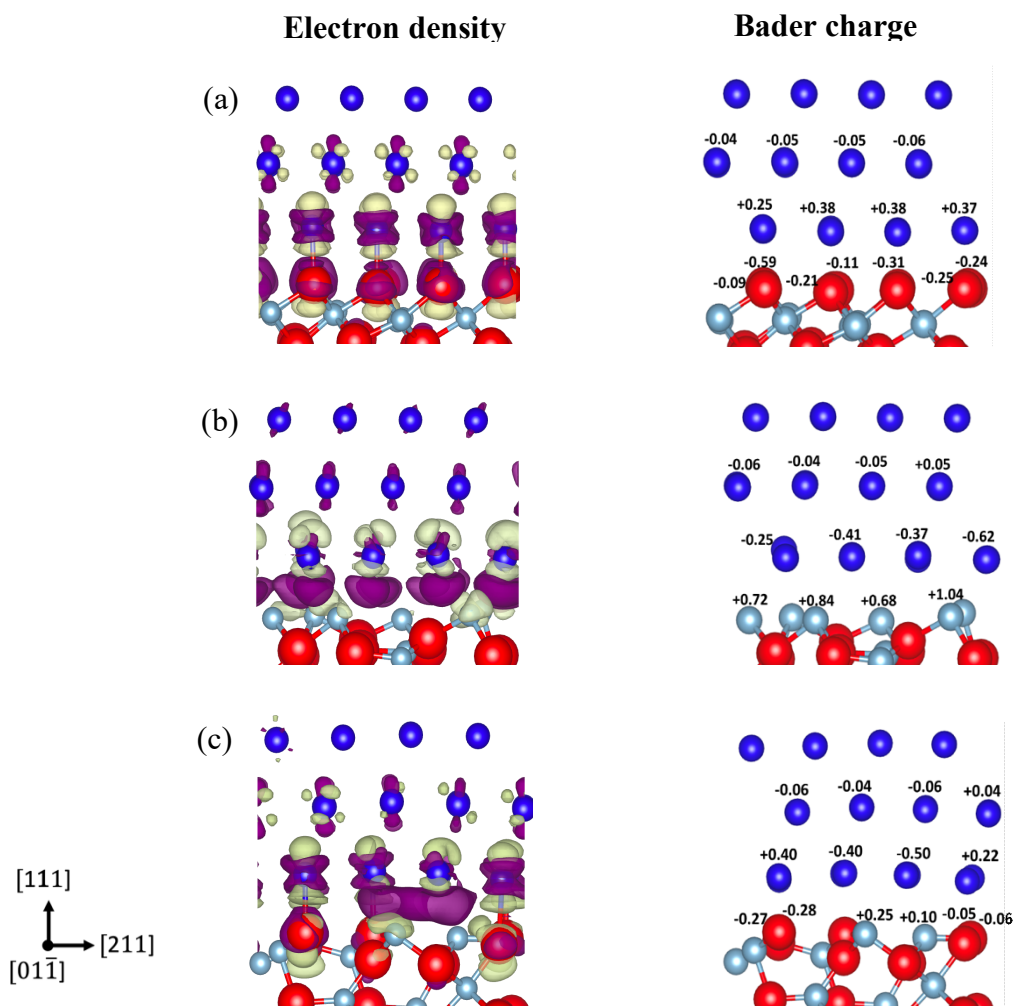








Fig. 7. The plot presents the difference in charge density distribution (CDD) and the difference in electronic charge of atoms at the interfacial plane of (a) O, (b) Al₂ and (c) Al terminations. The beige colored areas are positive CDD corresponding to regions of electron depletion and the dark-purple regions are negative CDD corresponding to electron accumulation. Isosurface value used for the Vesta[57] CDD plots are (a) 0.0055 (b) 0.0039 (c) 0.0044. A positive Bader charge change corresponds to electron loss and a negative change corresponds to electron gain. Pt, O and Al atoms shown in blue, red and light grey, respectively.

We examined the charge distribution profile (Fig. 8) along the thickness of the Pt metal slab to determine the extent to which the charge loss to the γ -Al₂O₃ support affects the electronic structure of the metal for the O-terminated interface. The Pt atoms at the interface show significant loss of electrons, but Pt atoms from the second layer and beyond show no significant changes in charge. This implies that the electronic effect of the γ -Al₂O₃ support on a Pt nanoparticle is largest at the interface and dissipates beyond the first couple of Pt layers.

Pt slab on $\gamma\text{-Al}_2\text{O}_3$ (O-termination)	Average charge
	0.0
	0.0
	-0.05
	-0.02
	+0.36
	-0.26

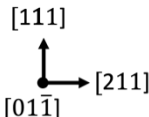


Fig. 8. The change in Bader charge, Δe , as a function of Pt atoms from the interface layer to the top layer in contact with the vacuum.

4. Conclusions

We used density functional theory and *ab initio* thermodynamics to study different surface facets and terminations of $\gamma\text{-Al}_2\text{O}_3$ and the Pt(111)/ $\gamma\text{-Al}_2\text{O}_3$ (111) interface. The most stable surface orientation is the $\gamma\text{-Al}_2\text{O}_3$ (100) while HRTEM from previous studies shows that a highly prevalent interfacial orientation is Pt(111)/ $\gamma\text{-Al}_2\text{O}_3$ (111). For this interfacial orientation, the DFT-calculated structural models and the interfacial phase diagram of the three interfaces (Al, O, Al₂) shows that the stability between the metal/metal-oxide interface correlates with the presence of metal-oxygen bonds at the interface. The most stable interface, over a wide range of temperature and oxygen pressures is O-terminated comprising of only electrostatic Pt-O bonds at the interface. With increasing temperature and decreasing oxygen partial pressure the Al-terminated interface which has fewer Pt-O bonds becomes stable, followed by the Al₂-terminated interface which has no Pt-O at the interface. These are consistent with previous studies showing that interactions at the metal-oxide interfaces are dominated by metal-oxygen bonds.[22]

The interfacial Pt atoms donate charge to the O but that interaction dissipates rapidly in underlying layers implying that the effect of the catalyst-support interactions on the catalyst electron structure is the largest at the interface with minimum effects on atoms above the interfacial layer. This study provides insights into the chemical bonding and the effects of temperature and oxygen pressure on metal/metal-oxide interfaces, essential for understanding metal-metal oxide interactions.”

Acknowledgements

This work was supported by the National Science Foundation, CER [Grant No. 1610507]. Part of the calculations used the Extreme Science and Engineering Discovery Environment (XSEDE)[62] (allocations TG-DMR160093 and TG-ENG170002) which is supported by National Science Foundation grant number ACI-1053575. The authors acknowledge the Texas Advanced Computing Center (TACC) at The University of Texas at Austin and the Comet cluster at the San Diego Supercomputer Center for providing HPC resources that have contributed to the research results reported within this paper. Electron microscopy was performed using the Titan TEM at the Center for Advanced Materials Characterization at Oregon (CAMCOR), which is supported by the Office of the Vice President of Research and Innovation of the University of Oregon.

References

- [1] D.R. Clarke, S.R. Phillpot, Thermal barrier coating materials, , Mater. Today, 8 (2005) 22-29.
- [2] H.L. Meyerheim, R. Popescu, J. Kirschner, N. Jedrecy, M. Sauvage-Simkin, B. Heinrich, R. Pinchaux, Geometrical and compositional structure at metal-oxide interfaces: MgO on Fe(001), Phys. Rev. Lett., 87 (2001).
- [3] H.-S. Chang, Y.-C. Chiu, C.-S. Yang, M. Chen, Oxide layer characteristics and interfacial analysis of porcelain fused to high-gold alloy using multitechnique analysis methods, J. Dent. Sci. (2017).
- [4] M. Lorenz, *et al.*, The 2016 oxide electronic materials and oxide interfaces roadmap, J. of Phys. D, 49 (2016).
- [5] G. Lan, Y. Jiang, D. Yi, S. Liu, Theoretical prediction of impurity effects on the internally oxidized metal/oxide interface: the case study of S on Cu/Al₂O₃, Phys. Chem. Chem. Phys., 14 (2012) 11178-11184.
- [6] O.M. Akselsen, Diffusion bonding of ceramics, J. of Mater. Sci., 27 (1992) 569-579.
- [7] P. Alemany, R.S. Boorse, J.M. Burlitch, R. Hoffmann, Metal-ceramic adhesion quantum-mechanical modeling of transition metal – Al₂O₃ interfaces, J. of Phys. Chem., 97 (1993) 8464-8475.
- [8] F. Ernst, metal-oxide interfaces, Mater. Sci. & Eng. R., 14 (1995) 97-156.
- [9] G. Feldbauer, M. Wolloch, P.O. Bedolla, P. Mohn, J. Redinger, A. Vernes, Adhesion and material transfer between contacting Al and TiN surfaces from first principles, Physical Review B, 91 (2015).
- [10] M.K. Santala, V. Radmilovic, R. Giulian, M.C. Ridgway, R. Gronsky, A.M. Glaeser, The orientation and morphology of platinum precipitates in sapphire, Acta Materialia, 59 (2011) 4761-4774.
- [11] E. Saiz, R.M. Cannon, A.P. Tomsia, High-temperature wetting and the work of adhesion in metal/oxide systems, in: Annual Review of Materials Research, 2008, pp. 197-226.
- [12] E. Saiz, R.M. Cannon, A.P. Tomsia, Energetics and atomic transport at liquid metal/Al₂O₃ interfaces, Acta Materialia, 47 (1999) 4209-4220.
- [13] J.G. Li, Wetting and interfacial bonding in liquid metal/solid ceramic systems, Composite Interfaces, 1 (1993) 37-53.
- [14] M. Backhaus-Ricoult, L. Samet, M.F. Trichet, M.J. Hytch, D. Imhoff, Interfacial chemistry in internally oxidized (Cu,Mg)-alloys, Journal of Solid State Chemistry, 173 (2003) 172-188.

- [15] M. Backhaus-Ricoult, Wetting anisotropy and oxygen activity dependency for oxides by liquid transition metals studied through shape changes of liquid Cu inclusions within MgO, *Acta Materialia*, 49 (2001) 1747-1758.
- [16] I.G. Batyrev, A. Alavi, M.W. Finnis, Equilibrium and adhesion of Nb/sapphire: The effect of oxygen partial pressure, *Physical Review B*, 62 (2000) 4698-4706.
- [17] J.W. Feng, W. Zhang, W. Jiang, Ab initio study of Ag/ Al₂O₃ and Au/ Al₂O₃ interfaces, *Physical Review B*, 72 (2005).
- [18] C. Kruse, M.W. Finnis, V.Y. Milman, M.C. Payne, A. De Vita, M.J. Gillan, First-Principles Calculations for Niobium Atoms on a Sapphire Surface, *Journal of the American Ceramic Society*, 77 (1994) 431-436.
- [19] C. Ophus, M.K. Santala, M. Asta, V. Radmilovic, Structure and phase transitions at the interface between alpha-Al₂O₃ and Pt, *Journal of Physics-Condensed Matter*, 25 (2013).
- [20] D. Siegel, L. Hector, J. Adams, Adhesion, atomic structure, and bonding at the Al(111)/alpha-Al₂O₃(0001) interface: A first principles study, *Physical Review B*, 65 (2002).
- [21] C.T. Campbell, J.R.V. Sellers, Anchored metal nanoparticles: Effects of support and size on their energy, sintering resistance and reactivity, *Faraday Discussions*, 162 (2013) 9-30.
- [22] S.L. Hemmingson, C.T. Campbell, Trends in Adhesion Energies of Metal Nanoparticles on Oxide Surfaces: Understanding Support Effects in Catalysis and Nanotechnology, *Acs Nano*, 11 (2017) 1196-1203.
- [23] K. Reuter, M. Scheffler, Composition, structure, and stability of RuO₂(110) as a function of oxygen pressure, *Physical Review B*, 65 (2001) 035406.
- [24] W. Zhang, J.R. Smith, Nonstoichiometric Interfaces and Al₂O₃ Adhesion with Al and Ag, *Physical Review Letters*, 85 (2000) 3225-3228.
- [25] A.L. Clauser, R. Giuliani, Z.D. McClure, K.O. Sarfo, C. Ophus, J. Ciston, L. Árnadóttir, M.K. Santala, Orientation and morphology of Pt nanoparticles in γ -alumina processed via ion implantation and thermal annealing, *Scripta Materialia*, 188 (2020) 44-49.
- [26] M. Backhaus-Ricoult, M.F. Trichet, Comparison of interfacial chemistry at Cu/alpha-alumina and Cu/gamma-alumina interfaces, *Zeitschrift Fur Metallkunde*, 94 (2003) 250-258.
- [27] M. Digne, P. Sautet, P. Raybaud, P. Euzen, H. Toulhoat, Use of DFT to achieve a rational understanding of acid-basic properties of gamma-alumina surfaces, *Journal of Catalysis*, 226 (2004) 54-68.
- [28] W.H. Lee, K.R. Vanloon, V. Petrova, J.B. Woodhouse, C.M. Loxton, R.I. Masel, The Equilibrium Shape and Surface-Energy Anisotropy of Clean Platinum, *Journal of Catalysis*, 126 (1990) 658-670.
- [29] G. Kresse, J. Hafner, Ab initio molecular dynamics for liquid metals, *Physical Review B*, 47 (1993) 558-561.
- [30] G. Kresse, J. Furthmüller, Efficiency of ab-initio total energy calculations for metals and semiconductors using a plane-wave basis set, *Computational Materials Science*, 6 (1996) 15-50.
- [31] G. Kresse, J. Hafner, Ab initio molecular-dynamics simulation of the liquid-metal--amorphous-semiconductor transition in germanium, *Physical Review B*, 49 (1994) 14251-14269.
- [32] G. Kresse, J. Furthmüller, Efficient iterative schemes for ab initio total-energy calculations using a plane-wave basis set, *Physical Review B*, 54 (1996) 11169-11186.
- [33] J.P. Perdew, K. Burke, M. Ernzerhof, Generalized Gradient Approximation Made Simple, *Physical Review Letters*, 77 (1996) 3865-3868.
- [34] G. Kresse, D. Joubert, From ultrasoft pseudopotentials to the projector augmented-wave method, *Phys. Rev. B*, 59 (1999) 1758-1775.
- [35] P.E. Blöchl, Projector augmented-wave method, *Physical Review B*, 50 (1994) 17953-17979.
- [36] H.J. Monkhorst, J.D. Pack, Special points for Brillouin-zone integrations, *Physical Review B*, 13 (1976) 5188-5192.
- [37] I. Levin, T. Gemming, D.G. Brandon, Some Metastable Polymorphs and Transient Stages of Transformation in Alumina, *physica status solidi (a)*, 166 (1998) 197-218.

- [38] L. Samain, A. Jaworski, M. Edén, D.M. Ladd, D.-K. Seo, F. Javier Garcia-Garcia, U. Häussermann, Structural analysis of highly porous γ -Al₂O₃, *Journal of Solid State Chemistry*, 217 (2014) 1-8.
- [39] A. Vijay, G. Mills, H. Metiu, Structure of the (001) surface of γ alumina, *Journal of Chemical Physics*, 117 (2002) 4509.
- [40] M. Trueba, S.P. Trasatti, γ - Alumina as a Support for Catalysts: A Review of Fundamental Aspects, *Eur. J. Inorg. Chem.*, 2005 (2005) 3393-3403.
- [41] M. Digne, P. Sautet, P. Raybaud, P. Euzen, H. Toulhoat, Use of DFT to achieve a rational understanding of acid– basic properties of γ -alumina surfaces, *Journal of Catalysis*, 226 (2004) 54-68.
- [42] X. Krokidis, P. Raybaud, A.-E. Gobichon, B. Rebours, P. Euzen, H. Toulhoat, Theoretical Study of the Dehydration Process of Boehmite to γ -Alumina, *The Journal of Physical Chemistry B*, 105 (2001) 5121-5130.
- [43] G. Paglia, C.E. Buckley, A.L. Rohl, B.A. Hunter, R.D. Hart, J.V. Hanna, L.T. Byrne, Tetragonal structure model for boehmite-derived γ -alumina, *Physical Review B*, 68 (2003) 144110.
- [44] Z. Song, B. Wang, J. Yu, C. Ma, Q. Qu, Z. Zeng, J. Xiang, S. Hu, L. Sun, Adsorption properties of CO, H₂ and CH₄ over Pd/ γ -Al₂O₃ catalyst: A density functional study, *Applied Surface Science*, 387 (2016) 341-350.
- [45] M. Digne, P. Sautet, P. Raybaud, P. Euzen, H. Toulhoat, Use of DFT to achieve a rational understanding of acid–basic properties of γ -alumina surfaces, *Journal of Catalysis*, 226 (2004) 54-68.
- [46] Y. Jiang, C. Xu, G. Lan, First- principles thermodynamics of metal- oxide surfaces and interfaces: A case study review, *Transactions Of Nonferrous Metals Society Of China*, 23 (2013) 180-192.
- [47] I. Batyrev, A. Alavi, M. W. Finnis, Abinitio calculations on the Al₂O₃(0001) surface, *Faraday Discussions*, 114 (1999) 33-43.
- [48] W. Bergermayer, H. Schweiger, E. Wimmer, Ab initio, *Physical Review B*, 69 (2004) 195409.
- [49] S.M. Kozlov, K.M. Neyman, Effects of electron transfer in model catalysts composed of Pt nanoparticles on CeO₂ (1 1 1) surface, *Journal of Catalysis*, 344 (2016) 507-514.
- [50] K. Anton, C. Mauro, Periodic density functional theory study of Pt(111): surface features of slabs of different thicknesses, *Journal of Physics: Condensed Matter*, 11 (1999) 7463.
- [51] P.J. Feibelman, B. Hammer, J.K. Nørskov, F. Wagner, M. Scheffler, R. Stumpf, R. Watwe, J. Dumesic, The CO/Pt(111) Puzzle, *The Journal of Physical Chemistry B*, 105 (2001) 4018-4025.
- [52] L.D.C. P. Villars, *Pearson's Handbook of Crystallographic Data for Inter-Metallic Phases*, 2nd ed., 1991.
- [53] W. Tang, E. Sanville, G. Henkelman, A grid-based Bader analysis algorithm without lattice bias, *Journal of Physics: Condensed Matter*, 21 (2009) 084204.
- [54] E. Sanville, S.D. Kenny, R. Smith, G. Henkelman, Improved grid-based algorithm for Bader charge allocation, *Journal of Computational Chemistry*, 28 (2007) 899-908.
- [55] G. Henkelman, A. Arnaldsson, H. Jónsson, A fast and robust algorithm for Bader decomposition of charge density, *Computational Materials Science*, 36 (2006) 354-360.
- [56] M. Yu, D.R. Trinkle, Accurate and efficient algorithm for Bader charge integration, *The Journal of Chemical Physics*, 134 (2011) 064111.
- [57] K. Momma, F. Izumi, VESTA 3 for three-dimensional visualization of crystal, volumetric and morphology data, *Journal of Applied Crystallography*, 44 (2011) 1272-1276.
- [58] I. Batyrev, A. Alavi, M.W. Finnis, Ab initio calculations on the Al₂O₃(0001) surface, *Faraday Discussions*, 114 (1999) 33-43.
- [59] J. Toofan, P.R. Watson, The termination of the α -Al₂O₃ (0001) surface: a LEED crystallography determination, *Surface Science*, 401 (1998) 162-172.
- [60] G. Jacek, F. Fabio, N. Claudine, Polarity of oxide surfaces and nanostructures, *Reports on Progress in Physics*, 71 (2008) 016501.
- [61] K. Wefers, C. Misra, *Oxides and Hydroxides of Aluminum: Alcoa Technical Paper No. 19, Revised in, Alcoa Laboratories, 1987.*

[62] J. Towns, T. Cockerill, M. Dahan, I. Foster, K. Gaither, A. Grimshaw, V. Hazlewood, S. Lathrop, D. Lifka, G.D. Peterson, R. Roskies, J.R. Scott, N. Wilkens-Diehr, XSEDE: Accelerating Scientific Discovery, *Computing in Science & Engineering*, 16 (2014) 62-74.